UNIVERSITATEA TEHNICĂ
DIN CLUJ-NAPOCA

Automatic Medium and High Earth Orbit Observation System Based on Stereovision (AMHEOS)

Progress Report, June 2013

Project Manager: Dr. Eng. Radu Danescu

Research teams:

CO-UTCN: Radu Danescu, Sergiu Nedevschi, Tiberiu Marita, Florin Oniga, Anca Ciurte
P1-BITNET: Octavian Cristea, Paul Dolea, Paul Dascal, Sebastian Cristea
P2-AROAC: Vlad Turcu, Tiberiu Oproiu, Alexandru Pop, Dan Moldovan, Liviu Mircea

Contents

1. Progress summary, June 2013

The first planned activity for 2013 is the enhancing of the accuracy of the optical system, so that higher distance objects can be observed. A comprehensive study of the available products on the market was performed, along with theoretical and experimental studies of accuracy. In the second half of the year the systems will be purchased and set up. The second planned activity is related to the automatic synchronization of the stereo system cameras. Experiments have been performed with new equipment, and the results confirmed the performance improvement. In the second part of the year the software drivers for integrating the synchronization boards in the AMHEOS system will be developed. The third task is related to the development of software tools for far range stereovision. Significant progress has been achieved towards the automatic detection of satellite streaks, and their accurate position estimation. Also, progress has been made towards automatic determination of camera parameters with minimum human intervention. Further efforts will be made towards increasing the precision of localization, matching and reconstruction, and towards achieving real time results.

2. Enhancing the accuracy of the optical system for increasing the detection distance

2.1. Estimation of the observation precision for the existing systems

Estimation of precision for one system
Twn existing systems:

2 Telescopes (D=150mm, F=750mm),

2 DSLR Canon EOS 50D (2352 x 1568 pixels) cameras, (9.4 μm x 9.4 μm) pixel size

Based on the tests performed on these tests, observing satellites of type MEO, HEO and GEO, and the astrometric reductions using two software packages (AIP4WIN V2.10 [1]; Astrometrica V 4.8.2.405 [2], [3]) we achieved comparable results for the precision of astrometric determination.

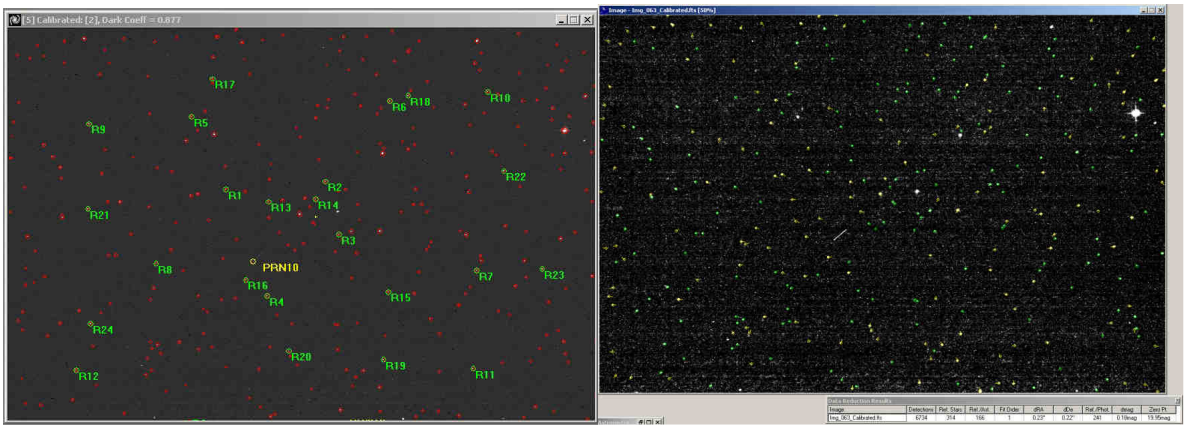

Fig. 1. Astrometric reductions for the same image, using AIP4WIN V2.0 (left), and Astrometrica V 4.8.2.405 (right), for a MEO type satellite (GPS PRN10), observed from the Marisel station.

The astrometric positioning precision for AIP4WIN V2.0, using 24 stars, was 0.339”, and for Astrometrica V 4.8.2.405, using 166 reference stars, was 0.225”. The angular size of the pixels is 2.5”.

The faintest magnitude of the sky objects that could be captured using a 5 seconds exposure was 19.9.

2.2. Estimation of the limits of the parameters of the system to be developed

Minimum focal distance, resolution and disparity for the two observation stations

The minimum resolution for the system to be developed is 1"/ pixel (arcsecond/ pixel) which means a distance resolution of 200m for HEO/GEO satellites, and 100 m resolution for MEO satellites. The equations for computing the focal distance, when the pixel size of the image sensor is known ($l_{pixel\ H} = l_{pixel\ V} = l_{pixel}$) and the angular resolution (α) are:

$$\tan\left(\frac{\alpha}{2}\right) = \frac{l_{pixel}}{2 \cdot F}$$

$$F \geq \frac{l_{pixel}}{2 \cdot \tan\left(\frac{\alpha}{2}\right)}$$

For a sensor of 9μm pixel size, we get a minimum focal distance of F=1856mm.

On the other hand, the separation between the observation stations (baseline) determines the limits of disparity (β) for the stereo image pair. For the most favorable case (the satellite is observed when passing through the mediator plane of the baseline), for the actual situation of our two observing stations (Feleac and Marisel, d=36.5 km), we get:

$$\beta \leq 2 \cdot \arctan\left(\frac{d_{Stereo}}{2 \cdot H_{satelit}}\right)$$

$$\beta_{GEO/HEO} \leq 188"$$

$$\beta_{MEO} \leq 376"$$

Combining the two conditions, we get the disparity values in pixels:

$$\beta_{GEO/HEO\ pixel} \leq 188 \text{ pixels}$$

$$\beta_{MEO\ pixel} \leq 376 \text{ pixels}$$

The focal distance must not, however, exceed a certain limit. This limit is imposed by the number of standard astrometric stars available in the field of view, and by the apparent speeds of the MEO, HEO and GEO satellites. The maximum focal distance must not exceed 4 m.

Aperture, faintest magnitude

The telescope's aperture (diameter) determines the faintest magnitude that can be observed. Increasing the magnitude (m) means that fainter objects can be detected (Pogson's equation):

$$m = -2.5 \cdot \log E + k$$

The flux E is proportional to the photon collecting surface, the main mirror of the telescope. Therefore, a higher maximum magnitude means a higher diameter of the telescope. On the other hand, the cost of the telescope increases with the diameter. The cost increase with the mirror's surface is depicted by the following equation [4]:

$$P = a \cdot S^{\gamma} + b$$

P is the price, S is the surface of the mirror, a and b are constants that depend on the manufacturer, and γ can have values between 1.1 and 2.5, depending on the manufacturer.

2.3. Estimation of the precision of observation for a system with similar parameters to the one to be developed

System: Meade RCX400 12" telescope (D=300mm, F=2400mm) + DSLR Canon EOS 50D camera, belonging to the Astronomical Observatory of the Babes Bolyai University of Cluj-Napoca.

A series of test observations for the relatively close pass of the Toutatis asteroid (7 milion km from Earth) was performed (fig. 2).

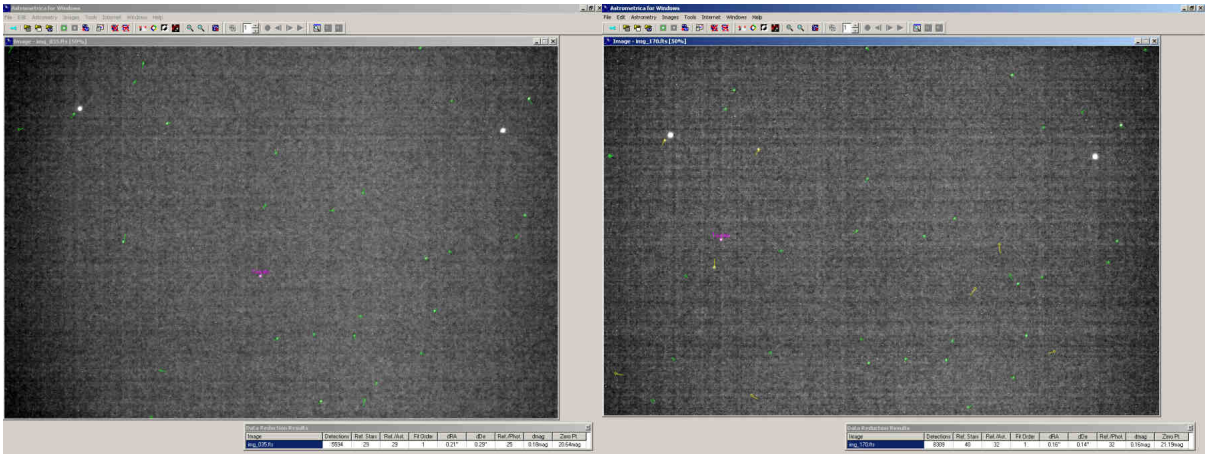

Fig. 2. Astrometric reductions for two images of the Toutatis observation series (date 13/12/ 2013).

The precision of astrometric positioning using 29 and 32 reference stars was 0.25" and, 0.15", respectively. The maximum observable magnitude, in urban sky conditions, was 20.6 mag, and 21.2 mag. The two images were chosen from the beginning (astronomical crepuscule) and the end of the observation series (better visibility). The covered field of view was 30.9' x 20.6', and the pixel resolution was 0.79"/pixel. Therefore, the tested system can be suitable for our project's desired performance requirements.

2.4. Possible telescope configurations and prices

a.	Meade LX200 8" ACF	Meade LX200 10" ACF	Meade LX200 12" ACF	Meade LX850 10" ACF	Meade LX850 12" ACF	Meade LX600 10" ACF	Meade LX600 12" ACF
Diameter D (mm)	203	254	305	254	305	254	305
Focal distance F (mm)	2000	2500	3000	2032	2440	2032	2440
Difraction limit	0.56"	0.45"	0.38"	0.457"	0.38"	0.457"	0.38"
Image field of view (Canon DSLR EOS 50D)	38'X25.33'	30'X20'	25.3'x16.9'	37'X25'	31'x21'	37'X25'	31'x21'
Accessories	-	-	-	Starlock +	Starlock +	Starlock +	Starlock

				Focus	Focus	Focus	+ Focus
Mount	Fork	Fork	Fork	German	German	Fork	Fork
Price (Euro)	3499	4799	5999	9999	11999	6240	7440
b.	Celestron CPC Deluxe 800 HD	Celestron CPC Deluxe 925 HD	Celestron CPC Deluxe 1100 HD	Celestron CGE Pro 925	Celestron CGE Pro 1100	Celestron CGE Pro HD 925	Celestron CGE Pro HD 1100
Diameter D (mm)	203	235	280	235	280	235	280
Focal distance F (mm)	2032	2350	2800	2350	2800	2350	2800
Difraction limit	0.57”	0.49”	0.42”	0.49”	0.42”	0.49”	0.42”
Image field of view (Canon DSLR EOS 50D)	38’X25.33’	32.3’X21.6’	27.1’x18.1’	32.3’X21.6’	27.1’x18.1’	32.3’X21.6’	27.1’x18.1’
Accessories	-	-	-	-	-	-	-
Mount	Fork	Fork	Fork	German	German	German	German
Price (RON)	2998	4220	5033	7997	8642	9067	9867

Table 1. a. Meade Instruments Telescopes [5], b. Celestron Telescopes [6]

Comparing the parameters and the performance of the telescopes presented in table 1, the solution of choice seems to be Meade LX600 12” ACF. This solution shows a focal ratio F/D = 8, which means an image field of view larger than a telescope with the same aperture but a focal ratio of 10 (Meade LX200 12”, or Celestron CGE 1100). The accessories than can be included in the price, and the compatibility with the adapters and accessories the consortium already has, are a major plus.

3. Development of an automatic system for synchronized acquisition of stereo images from far apart locations

Synchronization is crucial for stereovision, and for this reason experiments have been performed in order to find the best hardware solution for our system. As no high speed communication infrastructure can be set up between our two observation sites, we focused our attention on GPS receiving boards, having a high speed PCI interface and the capability of delivering the Pulse Per Second (PPS) signal. Thus, the delays that were previously introduced by the USB-connected low cost GPS receivers were drastically reduced.

In order to assess the synchronization quality and reliability, we have employed two FG6039GPS internal GPS receivers [7], installed on two desktop PCs. For evaluating the relative delay between the PPS signals of the two GPS receivers, a RIGOL DS5202MA digital oscilloscope was used. The setup of the experiment is shown in figures 3-7.

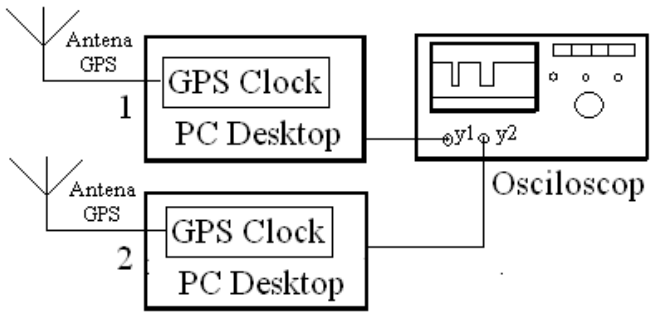

Fig. 3. Set up of the synchronization evaluation experiment.

Fig. 4. The antennas of the two GPS receivers, placed on the same pole.

Fig. 5. The equipment used for measuring the time delay.

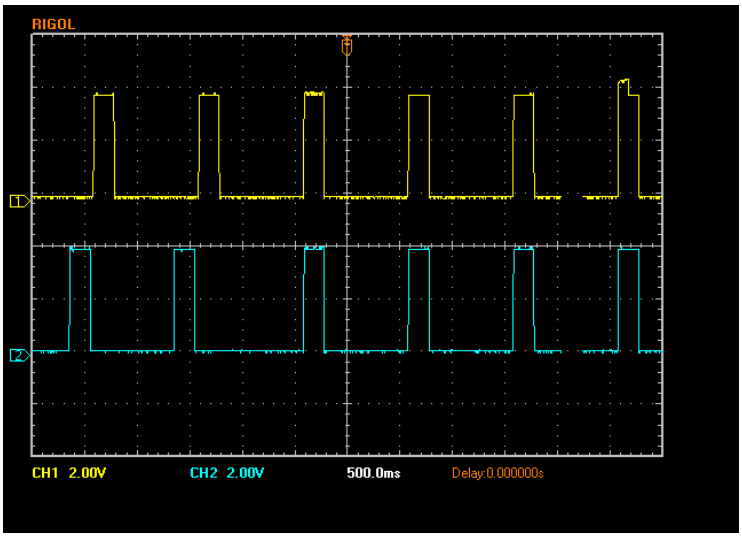

Fig. 6. Pulse trains generated by the two receivers. Oscilloscope time base is 500ms/div.

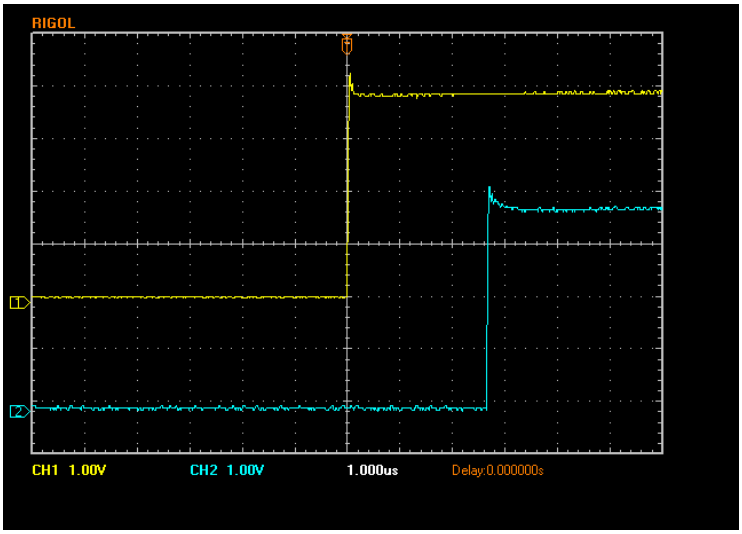

Fig. 7. Measuring the time delay, using a time base of 1μs/div. A time delay of approximately 2,8μs is observed.

Several measurement runs were performed, under different conditions:

- With GPS antennas set up such that the whole sky was visible
- With GPS antennas set up such that approximately 50% of the sky was visible
- Different times of day, with more or fewer GPS satellites visible

After analyzing the results, we observed that the time delay between the PPS pulses of the two GPS receivers did not exceed 3μs. Moreover, the capability of FG6039GPS receivers to generate single pulses at pre-programmed times makes them well suited for the needs of our system. The next step is to create a software interface between the receivers and the cameras, so that the stereo system can acquire well synchronized image pairs.

3. Development of stereovision software tools for high range measurement

3.1. Improvement of automatic detection of satellite streaks

The high distance satellites pose a significant challenge to an automatic detection system, due to low contrast, the presence of heavy noise, and the presence of high intensity stars in the satellite's neighborhood.

The defining characteristic of the satellite's appearance in the acquired images is their linear trajectory, which defines linear structures in the image, structures that we do not expect to obtain from other sources.

In order to detect linear objects with a relatively significant length, we propose a new method that consists in processing of block searching windows, using the Radon transform [8]. Because the intensity level of the satellites may vary significantly, and some satellites might appear very faint, we cannot afford any thresholding based preprocessing, such as the Hough transform [9], the classical detector for lines. The Radon transform is similar to Hough, but increments line space accumulators with the pixel intensities, for all pixels in the search window. Because the searching windows are small enough, the local maximum with the highest intensity value will, hopefully, correspond to a satellite.

A practical example is presented in the following figures follows. Given the original 2352x1568 pixels image shown in figure 8, the Radon transform is computed for all search windows within it. The search windows have a fixed size of 200x200 pixels, and are placed with a displacement step of 70 pixels, resulting in around 700 overlapped windows.

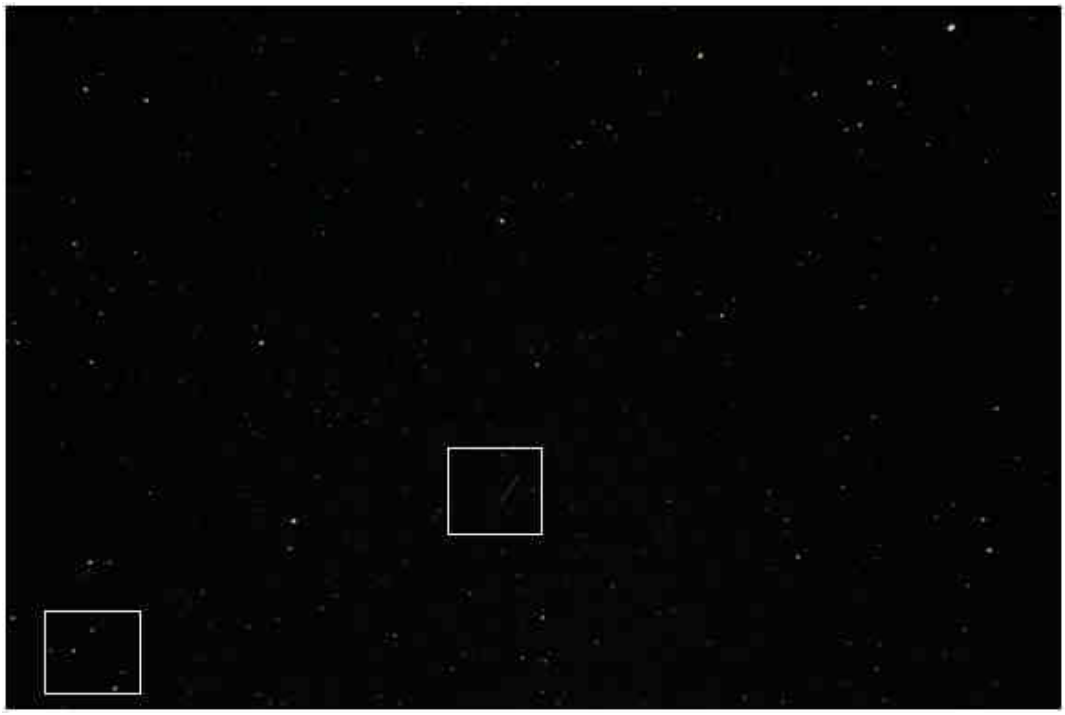

Fig. 8. Original acquired image and two search windows.

Figures 9 and 10 show intermediate processing results for the marked search windows of figure 8, corresponding to the two possible cases: satellite and no satellite.

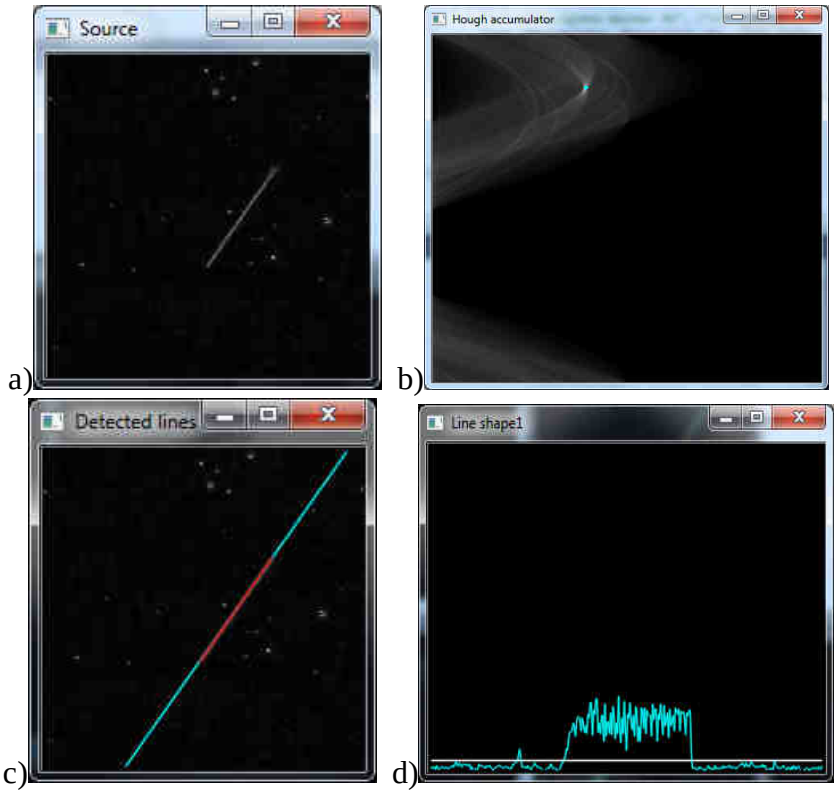

Fig. 9. A true satellite is detected.

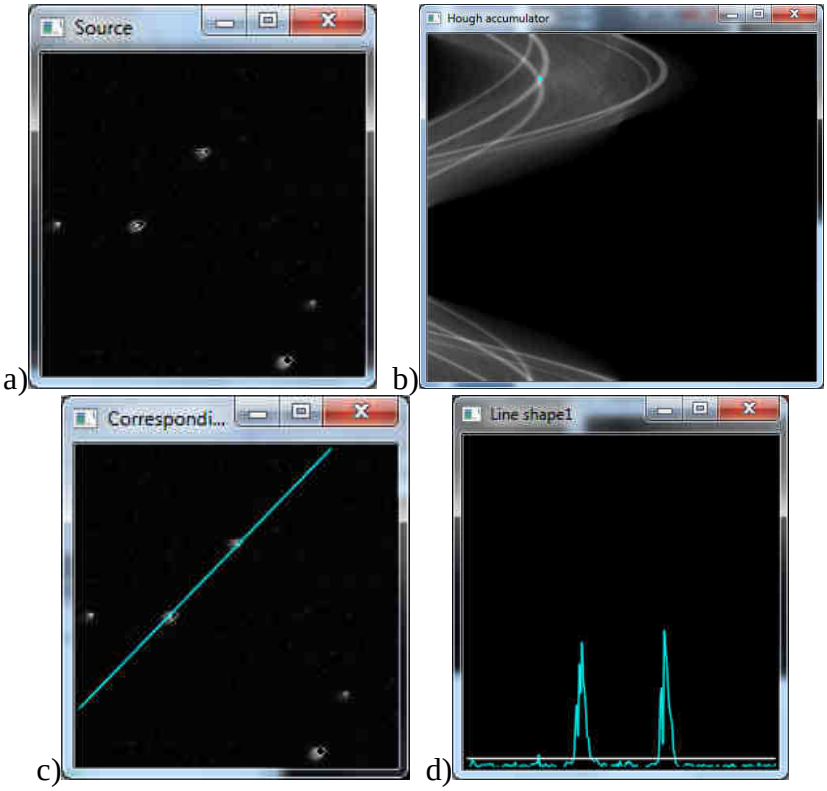

Fig. 10. A false positive is avoided.

In figures 9 and 10, sub-figures a) show the original search windows, and b) are the accumulator images (Radon transformed images). A point in the original image is represented as a sinusoid in the accumulator space, and a line in the original image is represented as a point. We look for the local maximum with highest intensity in the accumulator space (marked with a cyan point), and we reconstruct its corresponding line in the original image (figures c). The intensity values of the line points (the intensity profile of the line) are then plotted in sub-figures d). The condition for a satellite hypothesis to be validated is that more that 60 consecutive points on the detected line have an intensity value above the median of the searching window. In figure 9, the intensity profile of the line clearly shows a valid satellite, while in figure 10 the intensity profile shows two spikes corresponding to the two bright stars. The validated satellite is marked with red on sub-figure 9.c.

Other processing results are shown in figures 11 to 13. The last three examples show the robustness of the proposed method with respect to different levels of contrast between the satellite and the background.

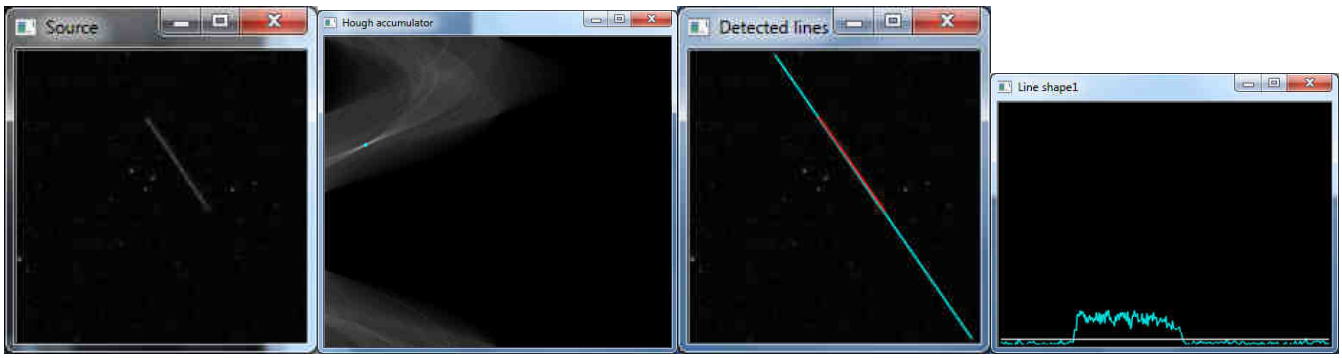

Fig. 11. Another example, for a different orientation.

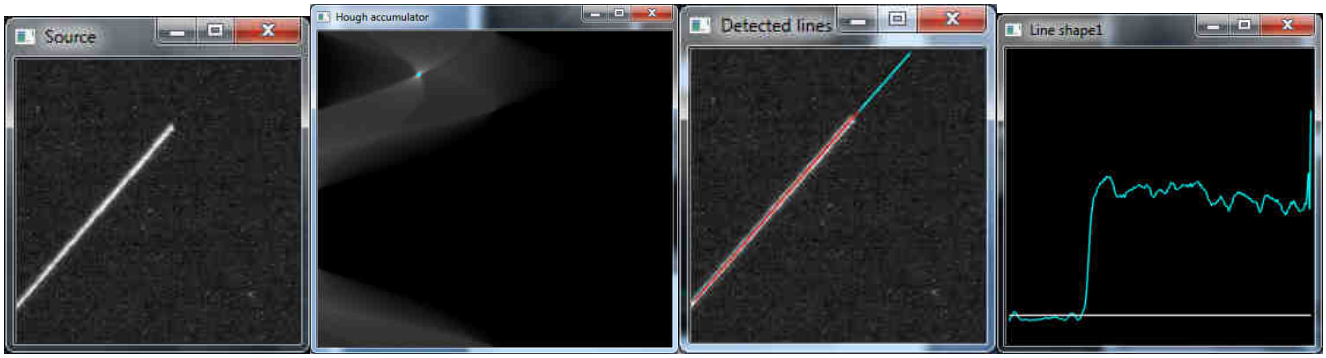

Fig. 12. Rotating satellite – high contrast phase.

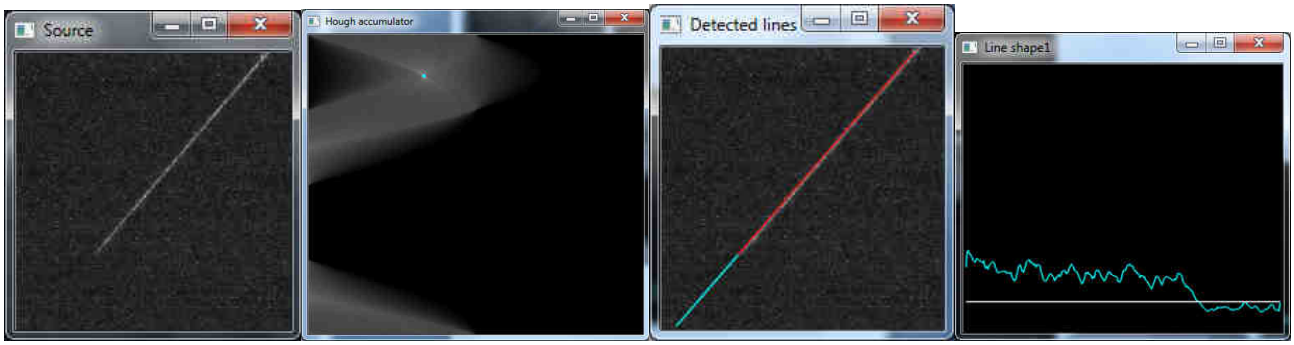

Fig. 13. Rotating satellite – medium contrast phase.

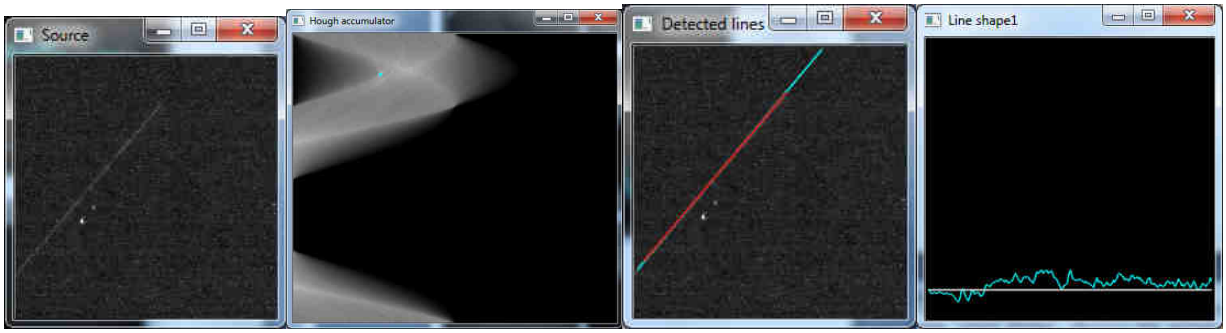

Fig. 14. Rotating satellite – low contrast phase.

Further experiments will be performed in order to improve the accuracy of the proposed method.

3.2. Increasing the accuracy and speed of the stereo-based 3D reconstruction

In order to achieve a fully automatic stereovision reconstruction engine, we have to continuously adjust the orientation parameters of the cameras with respect to the Earth-bound coordinate system. For this reason, calibration stars are tracked frame to frame, and the camera parameters are re-adjusted. In the previous year, we have developed a method to automatically fit the calibration stars to the image, when a reference image containing the pixel positions of the stars was available.

The new development goes towards removing the reference frame and the reference initial pixel positions of the calibration stars. The new solution is based on the following steps:

- Starting from the stellar coordinates RA and DEC, we create a virtual image of the calibration star field, using the known focal distance of the optical system.

- The virtual image of the star field is rotated and translated such that the sum of the intensities of the pixels corresponding to the stars becomes maximum.
- The individual positions of the stars are refined locally.

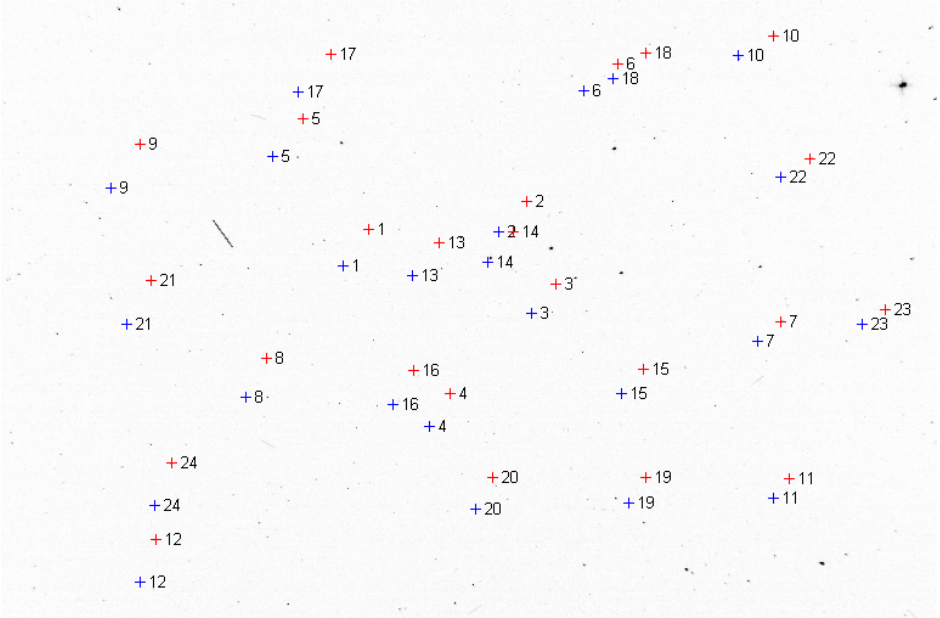

Fig. 15. Fitting the calibration stars without the need of initial control points

The preliminary results show that the method works for all our sequences. This way, a cumbersome human task can be removed from the system, and we made another significant step towards a completely automated identification of the stars, when only the approximate region of the sky that the telescope points towards is known. The future work will include the automatic extraction of the relevant calibration stars from an offline or an online star catalog, based on the orientation of the telescope.

4. Experiments

ROMANIAN PARTICIPATION TO EXPERIMENTS IN THE FRAMEWORK OF NATO STO SET-147 RTG (https://www.cso.nato.int/ACTIVITY_META.asp?ACT=1717)

Activity: Ground-based, multi-sensor observations of NEOSSAT
Target: detect and identify NEOSSAT within the satellites group of PSLV-C20 launch in the LEOP (Launch and Early Operation) phase.
Outcome: DONE !
Sample data: NEOSSAT streak as observed from Romania on 02.03.2013

TIME: not for public release.
Observations made from the Astronomical Observatory Cluj - "Babes-Bolyai" University station:

Longitude: 23 35 17.125 East
Latitude: 46 45 28.958 North
Elevation: 426 meters
Instrument:
Orion telescope: D=80mm, F=400mm
Canon EOS 50D DSLR type camera
FOV approximately 3 degrees x 2 degrees

Timing was insured with an external trigger synchronized with a GPS receiver (via microcontroller board). Exposure time was 1.3 sec.

The observed zone was centered on SAO 54074, near M31 (Andromeda galaxy). Due to the short exposure times, the spiral arms of the galaxy are invisible, and the central bulge is just outside of the image - upper side.

5. Dissemination of preliminary results

So far, two ISI papers have been published:

1. R. Danescu, F. Oniga, V. Turcu, O. Cristea, “Long Baseline Stereovision for Automatic Detection and Ranging of Moving Objects in the Night Sky”, *Sensors*, vol. 12, No. 10, October 2012, pp. 12940-12963. [**most recent impact factor: 1.95**]
2. O. Cristea, P. Dolea, V. Turcu, R. Danescu, “Long baseline stereoscopic imager for close to Earth objects range measurements”, *Acta Astronautica*, vol. 90, No. 1, September 2013, pp. 41-48. [**most recent impact factor: 0.701**].

Two diploma and master theses have been written:

1. Claudiu Ban, “Abordare paralela pentru detectia satelitilor din imagini”, Master Thesis, UTCN, 2013 (supervisor, R. Danescu).
2. Emanuel Comes, “Sistem de extragere a trasaturilor relevante pentru procesul de supraveghere optica de la sol a orbitelor terestre medii (MEO)”, Diploma work, UTCN, 2013 (supervisor, R. Danescu).

References

[1] Berry, R., Burnell, J., 2005, *The Handbook of Astronomical Image Processing. Second Edition* Willmann-Bell, Inc., Richmond, Virginia, USA

[2] Raab, H., 1993-2013, *Astrometrica,* http://www.astrometrica.at

[3] Raab, H., 2002, *Detecting and measuring faint point sources with a CCD,* Meetings on Asteroids and Comets in Europe, May 17-19,2002, Visnjan, Croatia, MACE 2002 Proceedings , pp.12-17, http://www.astro.hr/mace2002/Report/MACE2002_final.PDF

[4] Turcu, V., 2010, *Contribuții asupra metodelor de achiziție și prelucrare ale semnalelor în astronomie. Teză de doctorat,* Universitatea Tehnică din Cluj-Napoca

[5] * * * Meade Instruments Corporation, 2013, http://www.meade.com

[6] * * * Celestron LLC., 2013, http://www.celestron.com

[7] HOPF Elektronik – Technical Description PC satellite clock 6039 GPS, 2011, [Online]: http://www.hopf-time.com

[8] Deans, Stanley R. (1983), *The Radon Transform and Some of Its Applications*, New York: John Wiley & Sons

[9] Duda, R. O. and P. E. Hart, "Use of the Hough Transformation to Detect Lines and Curves in Pictures," *Comm. ACM, Vol. 15*, pp. 11–15 (January, 1972)